Hindawi
Concepts in Magnetic Resonance Part A, Bridging Education and Research
Volume 2023, Article ID 7642095, 9 pages
https://doi.org/10.1155/2023/7642095

Research Article

Multislice B_1 Mapping Method Using Magnetic Resonance Composite Spin Echo Sequences and Simultaneous Echo Refocusing

Suchit Kumar,[1] **Kyu Chan Lee**,[2] **Jong-Min Kim**,[1] **Jeung-Hoon Seo**,[3] **Chulhyun Lee**,[4] **and Chang-Hyun Oh**[1,5]

[1]*Research Institute for Advanced Industrial Technology, Korea University, Sejong 30019, Republic of Korea*
[2]*Department of Radiation Oncology, Gil Medical Center, Gachon University College of Medicine, Incheon 21565, Republic of Korea*
[3]*Neuroscience Research Institute, Gachon University, Incheon 21988, Republic of Korea*
[4]*Bioimaging Research Team, Korea Basic Science Institute, Cheongju 28119, Republic of Korea*
[5]*Department of Electronics and Information Engineering, Korea University, Sejong 30019, Republic of Korea*

Correspondence should be addressed to Chang-Hyun Oh; ohch@korea.ac.kr

Received 10 November 2022; Revised 15 March 2023; Accepted 8 April 2023; Published 13 April 2023

Academic Editor: Yi Wang

Radiofrequency (RF) transmit field (B_1) mapping is a promising method in mitigating the B_1 inhomogeneity in various magnetic resonance imaging (MRI) applications. Although several phase- or magnitude-based B_1 mapping methods have been proposed, these methods often require complex modeling, long acquisition time, or specialized MRI sequences. A recently introduced simultaneous echo refocusing (SER) technique can be applied in the B_1 mapping method to extend the three-dimensional (3D) spatial coverage only without long data acquisition. Therefore, in this study, a multislice B_1 mapping method using composite spin echo sequences and SER techniques is proposed to obtain more accurate B_1 mapping with short data acquisition time. To evaluate the performance of the proposed B_1 mapping method, computational simulations were performed and compared with Morrell's method, double angle method, and Yarnykh's method. These results showed that the angle-to-noise ratio of the proposed B_1 mapping method has wider B_1 range compared to that of other B_1 mapping methods. In addition, the proposed B_1 mapping methods were compared to the multislice iterative signal intensity mapping method in both phantom and in vivo human experiments, and there was no remarkable difference between the two methods regarding the flip angle distribution in these experiments. Based on these results, this study demonstrated that the proposed B_1 mapping method is suitable for accurately measuring B_1 propagation under the condition providing reduced scan time and wider 3D coverage of B_1 mapping by applying composite RF pulse and SER techniques into the phase-sensitive method.

1. Introduction

Radiofrequency (RF) transmit field (B_1) measurement is used in various magnetic resonance imaging (MRI) applications, such as the adjustment of transmit gain to generate RF pulses for specific flip angle (FA), design of multitransmit RF pulses [1–3], specific absorption rate (SAR) estimation, and quantitative T_1 mapping [4, 5]. Several methods have been proposed to measure the RF B_1, which can be broadly classified into MR signal magnitude-based methods that estimate the B_1 from the magnitude of the MR image [6–15] and MR signal phase-based methods that estimate the B_1 from the phase of the MR image [16–19].

The magnitude-based B_1 mapping methods depend on changes in magnitude of MR signal according to the B_1 field and include fitting progressively increasing FAs [6], stimulated echoes [7], ratios of MR signals [8–12], signal null at certain FAs [13], ratio of the MR signals acquired at a dual steady state [14], and comparison of spin echo (SE) and stimulated echo signals [15]. These methods have several

combinations of the following problems: T_1 dependence; long acquisition times, mainly from acquiring several images; long repetition time (TR) for mitigating the T_1 acquisition; and inaccuracy over a wide range of B_1 especially at low FAs or FAs close to 90° or 180°. Several phase-based B_1 mapping methods have been proposed as an alternative to magnitude-based B_1 mapping methods [16–20]. To generate the MR signal phase dependence on FA, Morrell [16] and Chang [17] proposed the use of a pair of successive orthogonal RF pulses, whereas Sacolick et al. [18] proposed the use of the Bloch–Siegert phase shift effect [21].

Although such effective B_1 mapping methods based on phase or magnitude imaging have been proposed [7, 9, 11, 13–16, 18, 22–25], these methods often require the complex modeling, long acquisition time, or specialized MRI sequences. Therefore, these methods have not been integrated into clinical applications, resulting in an ongoing need for a practical, accurate, and fast B_1 mapping method.

The multislice excitation technique is commonly used in MRI to obtain three-dimensional (3D) spatial coverage. It can be described as a process during which multiple image planes are independently sampled using different frequency offsets in the RF pulses of otherwise identical MR pulse sequences. Experiments to improve efficiency in sequences for SE imaging have been demonstrated using interleaved methods. The interleaved T_2-weighted SE sequences where selective RF pulses independently excite and then refocus different slice signals, essentially interleaving the SE sequences during the delay time between pairs of excitations and refocusing pulses, have been successfully applied in clinical practice [26]. The multislice sequences are faster and more efficient than conventional analogs since the interleaving process eliminates relatively large sequence dead time. Recently, the simultaneous echo refocusing (SER) technique has been proposed to overcome the interleaved approaches [27]. The MR signals in multiple image planes are generated with slice-selective RF excitations and acquired within an SE pulse, utilizing a shared refocusing process. The MR signals originating from different slices are refocused at different times on each read period and further refocused with switched read gradients. In the proposed applications, temporal simultaneity of SER is effectively similar to that in 3D Fourier transform (FT) imaging, only without long data acquisition periods needed in 3D FT to obtain sufficient sampling along two-phase encoding axes. Therefore, the SER method can be used in the B_1 mapping method to extend the 3D spatial coverage only without long data acquisition. Particularly, the B_1 mapping method using composite RF pulses and multislice imaging (by applying SER techniques) is more efficient in reducing data collection time compared to the previous B_1 mapping method using composite RF pulses.

In this study, we proposed the multislice B_1 mapping method using a pair of composite RF pulses, $90_y^\circ - 0_x° - 90_y°$ and $90_y^\circ - 180_x° - 90_y°$, and SER technique. The performance of the proposed B_1 mapping method was evaluated using the computational simulations and phantom and *in vivo* human experiments using a 3-Tesla MRI scanner. Particularly, the multislice iterative signal intensity (ISI) mapping method was selected as a reference method for comparison with the proposed B_1 mapping method in all MR experiments because it is an accurate method for signal intensity measurements even if the data acquisition time is long [6].

2. Theory

2.1. Phase-Based B_1 Mapping Methods. As mentioned above, there are some phase-based B_1 mapping methods. One method by Oh is referred to as the SE phase-sensitive method [19]. This method uses composite SE pulses for encoding the FA in the phase of the resulting image and requires a baseline subtraction image for removing other sources of image phase, such as main magnetic field (B_0) inhomogeneity and receive phase. One method by Morrell is referred to as the phase-sensitive method [16]. This method uses an excitation pulse with a gradient-recalled echo (GRE) sequence for encoding the FA in the phase of the resulting image instead of using an SE sequence. This method has the same long TR requirement as the signal magnitude-based sequences, although it is effective and more accurate in a larger range of FAs than a double angle signal magnitude-based B_1 map [28]. These two phase-based B_1 mapping methods are based on composite RF pulses and typically employ large FAs. One method by Sacolick introduced the Bloch–Siegert shift method as an alternative to the composite RF pulse methods [18]. The Bloch–Siegert shift method provides a detectable phase shift in FA mapping, enabling the use of sufficiently long off-resonance RF pulses with amplitudes compatible with various clinical applications. The efficiency of the Bloch–Siegert shift method is insufficient due to the long RF pulse that requires a long echo time. One method by Chang requires a regular 3D GRE sequence with a magnetization preparation RF pulse of the same FA but orthogonal in phase to the excitation RF pulse for mapping the amplitude of the B_1 of a transmit RF coil in 3D [17].

2.2. Multislice B_1 Mapping Using a Pair of Composite RF Pulses and SER Technique. Figure 1 shows the pulse sequence diagram for the proposed B_1 mapping scheme. The pulse sequences begin with temporally sequential slice-selective RF pulses with selection gradients to produce signals in multiple adjacent slices. After temporally sequential selective RF pulses, a nonselective composite RF pulse of $90_y^\circ - 180_x° - 90_y°$ for sequence 1 and nonselective composite RF pulse of $90_y^\circ - 0_x° - 90_y°$ for sequence 2 are applied to generate the SE signals. Encoding gradients are also applied. Let us assume that the resulting magnetization for k-th slice-selective RF pulse is represented by $M_{re}^k(B_1;t) + iM_{im}^k(B_1;t)$. The resulting complex-numbered signal can be expressed as follows [19]:

$$S^k(B_1;t) = S_{re}^k(B_1;t) + iS_{im}^k(B_1;t), \tag{1}$$

and $S_{\text{seq1}}^k(B_1;t)$ and $S_{\text{seq2}}^k(B_1;t)$ are the resulting signals generated by the k-th slice-selective RF pulse with selection gradient of sequences 1 and 2, respectively.

These SE signals are acquired within each readout period and provide phase information that is dependent on the B_1

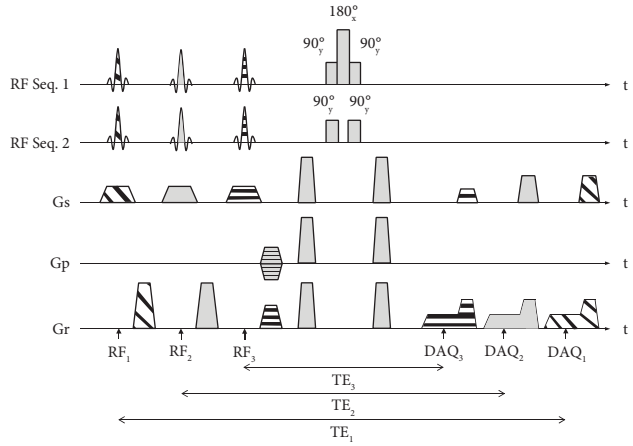

FIGURE 1: Multislice B_1 mapping method using RF pulses of 90_y° – 180_x° – 90_y° for sequence 1 and 90_y° – 0_x° – 90_y° for sequence 2.

field strength. The resulting phase of the k-th slice, ϕ_{B1}^k, can be obtained by calculating the phase difference of two pulse sequences:

$$\phi_{B1}^k = \text{phase}\left(S_{\text{seq1}}^k(B_1;t) \bullet \text{conj}\left(S_{\text{seq1}}^k(B_1;t)\right)\right), \quad (2)$$

where phase$(\circ)$ is the phase of argument and conj$(\circ)$ is the complex conjugate of argument. Because the phase difference between sequences 1 and 2 is identical except the RF-dependent phase change due to the 180_x° RF pulse, the proposed B_1 mapping method effectively eliminates all possible phase errors caused by other sources (e.g., RF coil-dependent phase delays). Although the phase change is directly proportional to the B_1 strength in first-order approximation, an B_0 inhomogeneity affects the application of nonselective composite RF pulse. Therefore, computational simulations are required to properly analyze the detailed spin behavior during the nonselective composite RF pulse. Practically, since B_0 inhomogeneity is dependent on the length of nonselective composite RF pulse, this length should be minimized. In this study, the Bloch equation for detailed spin behavior was solved using the fourth-order Runge–Kutta method [19]. After predicting the B_1field-dependent phase changes for a given B_0 inhomogeneity, the resulting phase behavior can be used to correct B_0 inhomogeneity of the proposed B_1 mapping method. An experimental B_0 inhomogeneity can be calculated using the echo-shifting method [19]. Therefore, two MR images were acquired with RF pulses of 90_y° – 180_x° – 90_y° and 90_y° – 180_x° – 90_y° with a shift of 1 ms. B_0 inhomogeneity effects in the resulting phase can be corrected based on the computational simulations.

3. Materials and Methods

The proposed B_1 mapping method is based on a phase-sensitive method and capable of acquiring multislice images. To evaluate the performance of the proposed B_1 mapping method, computational simulations were conducted, and it was compared with three other B_1 mapping methods: Morrell's method [16], double angle method (DAM) [11], and Yarnykh's method [14] (see Figure 2). For DAM based on the SE sequence, a simulation parameter was selected with two given FA values (90° and 180° for α and 2 α, respectively), to obtain two signal intensity maps (see Figure 2(a)), which involves 1% white Gaussian noise. Then, two signal intensity maps were calculated using equation (1), and the actual FA maps were measured at angles from 0° to 360°. For Yarnykh's method, the simulation parameters were selected with $TR_1/TR_2 = 100\,\text{ms}/400\,\text{ms}$ and $T_1 = 600\,\text{ms}$, and 1% white Gaussian noise was also used (see Figure 2(b)). Morrell's method was generalized to arbitrary FAs ($2\alpha_x$ and α_x) (see Figure 2(c)). If two orthogonal pulses of arbitrary, identical FAs are applied in quick succession, the FA would be estimated by $\alpha = \arccos(\tan(\theta))$, where θ is the resulting phase. The proposed B_1 mapping method was based on the phase sensitivity map (see Figure 2(d)). The phase maps were obtained using the Bloch equations [19]. The actual FA maps were calculated in a manner similar to Morrell's methods (i.e., $\text{FA}(\theta) = I_2(\theta) - I_1(\theta)$) using two-phase maps. In computational simulation, the signal-to-noise ratio (SNR) efficiency, which is indicated as the angle-to-noise ratio (ANR), was defined as the SNR in the FA map. For initial simulation comparison, readout acceleration along the phase encoding was not considered, and the optimal parameters that rely on the T_1 value of the tissue, target FA value, and T_2 effects were also ignored.

The study protocol was approved by the Institutional Review Board of the Korea University, and all procedures used in the study were conducted in accordance with the International Ethics Standards and the Declaration of Helsinki. Written informed consent was obtained from one participant (sex, male; age, 30 years) after a full explanation of the study procedures. The RF pulse sequence was designed with sequence secure data transfer software (Phillips Healthcare, Netherlands). To validate the signal intensity of the proposed B_1 mapping method, all MR experiments were performed in a 3-Tesla MRI scanner (Achieva TX, Philips Healthcare, The Netherlands) using two B_1 mapping methods: proposed B_1 mapping method and multislice ISI mapping method [6].

These methods were compared with the following parameters: TR/TEs = 500 ms/20 ms, 40 ms, and 60 ms; field of view = $240 \times 240\,\text{mm}^2$; matrix size = 560×560; number of slices = 3; slice thickness = 5 mm; FAs of temporally sequential excitations = 90°(α); and scan time = 4 : 01.5 per RF pulse (total acquisition time = 8 : 03). The multislice ISI mapping method was conducted by changing the FA of the refocusing pulse from 5° to 145° on the multislice SE with the same parameter resulting in scan time = 4 : 01.5 per FA (total acquisition time = 116 : 43.5), and the FA with the maximum signal was obtained via spatial mapping of the image. A water phantom consisting of $CuSO_4$ and distilled water (1 g/1 L) with a diameter and height of 200 mm was used in the phantom experiment. A commercial quadrature transmit/receive volume coil (Philips Healthcare, The Netherlands) was used in all MR experiments.

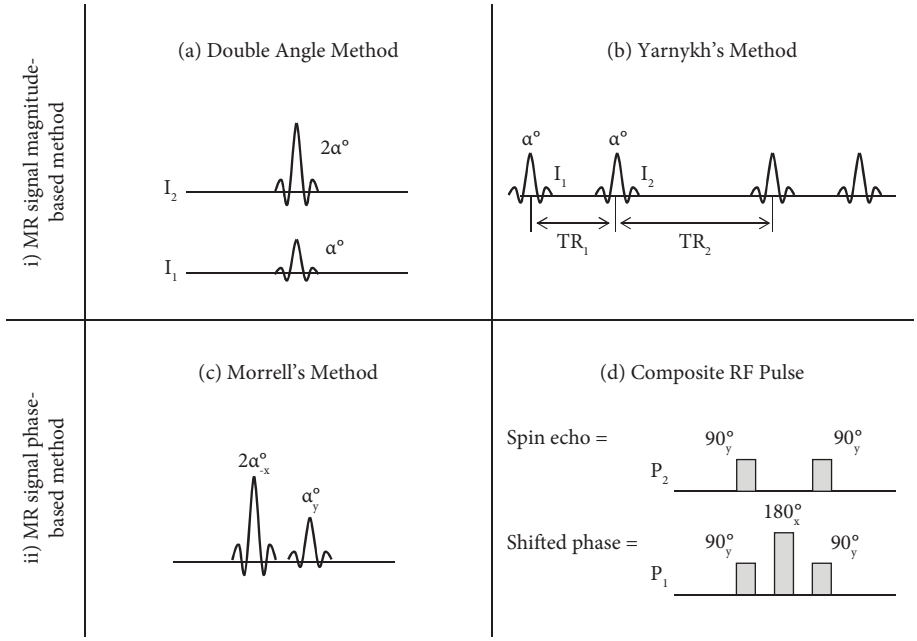

Figure 2: Computational simulation studies to evaluate the proposed B_1 mapping method using a composite RF pulse (d) and other B_1 mapping methods, such as the double angle method (a), Yarnykh's method (b), and Morrell's method (c).

4. Results

The resulting phase of the proposed B_1 mapping method from the numerical result for each RF field strength, B_0 inhomogeneity, and composite RF pulse duration is shown in Figure 3. Without B_0 and B_1 field inhomogeneities, the applied RF field strength and resulting phase are identical (180°). Without B_0 inhomogeneity, the obtained results show the quite linear RF field and resulting phase relationship within the given RF field strength range of [120°, 240°] without affecting the composite RF pulse duration. For a given B_0 inhomogeneity, the nonlinearity of the relationship between the resulting phase and RF field strength increased with increasing B_0 inhomogeneity. By considering RF power and B_0 inhomogeneity, a reasonable composite RF pulse duration for the phantom and *in vivo* human experiments is 300 μs, which makes the linear RF field and resulting phase relationship within the given RF field strength range of [120°, 240°].

Figure 4 shows the simulation results of ANR profiles for four B_1 mapping methods, including DAM, multislice composite RF pulse (proposed B_1 mapping method), Morrell's method, and Yarnykh's method. The ANR distribution of Yarnykh's method shows a bell-shaped curve, and the noise value changed at an FA of 180°. The ANR distributions of the DAM and Morrell's method show that their noise values increase at FAs of 47° and 3°, respectively. For the proposed B_1 mapping method, the noise value increases at an FA of 21°. Although the proposed B_1 mapping method did not create a large difference compared with Morrell's method (see Figure 4), these results clearly show that the ANR distribution of the proposed B_1 mapping method is more uniformly distributed compared to that of other B_1 mapping methods, indicating that the proposed B_1 mapping method could provide a more accurate FA value over a wider FA range. Moreover, in terms of scan efficiency, it should be noted that the proposed method performs 93.1% better than the multislice ISI mapping method.

Figure 5 shows MR magnitude images for three echo signals (RF_1, RF_2, and RF_3) obtained from the composite RF pulses in the phantom. Especially, the first row represents MR images by the RF sequence using a composite RF pulse ($90_y^\circ - 0_x^\circ - 90_y^\circ$), the second row shows MR images by the same RF sequence using a composite RF pulse ($90_y^\circ - 180_x^\circ - 90_y^\circ$) under the phase shift of 180° RF pulse on the x-axis, and the third row presents MR images by the RF sequence using a composite RF pulse ($90_y^\circ - 180_x^\circ - 90_y^\circ$) with 1 ms shift. Additionally, slices 1, 2, and 3 were obtained at different TEs of 30 ms, 20 ms, and 10 ms, respectively.

Figure 6 shows the FA distributions of the proposed B_1 mapping method and multislice ISI mapping method with the phantom. Figure 6(a) shows B_0 inhomogeneity maps estimated by RF sequence 1 using a composite RF pulse with 1 ms shift and RF sequence 1 using a composite RF pulse. The B_1 map estimated by the proposed B_1 mapping method with the no-correction method is shown in Figure 6(b). Based on computational simulations, phase maps generated by the proposed B_1 mapping method (see Figure 6(b)) are corrected with B_0 inhomogeneity (see Figure 6(c)). The difference between the values after and before correcting B_0 inhomogeneity is shown in Figure 6(d). Furthermore, the B_1 map estimated by a reference method, multislice ISI mapping method, is presented in Figure 6(e). Errors between the proposed B_1 mapping method and multislice ISI method are shown in Figure 6(f). There was no remarkable difference between the two methods regarding the FA distribution with the phantom (<10%). The main differences between the two

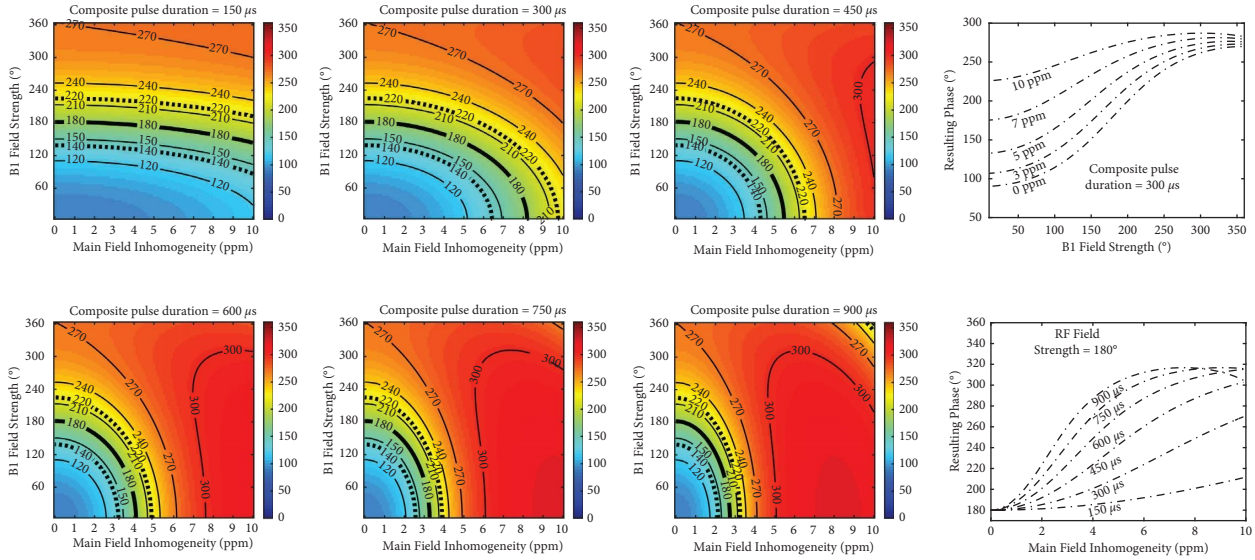

FIGURE 3: Phase differences of two MR images obtained from two composite RF pulse sequences according to B_1 field strength, B_0 inhomogeneity, and composite RF pulse duration. This contour graph was obtained by solving the Bloch equation numerically.

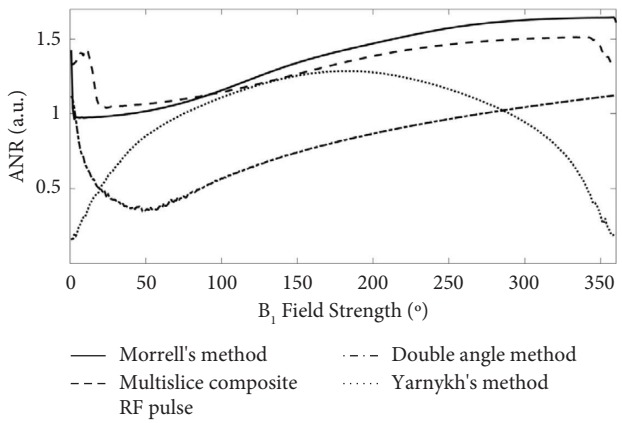

FIGURE 4: One-dimensional angle-to-noise ratio profiles of the single slice acquisition for the double angle method, multislice composite RF pulse method (proposed B_1 mapping method), Morrell's method, and Yarnykh's method.

methods are caused by the discrete patterns, which are created because the images are acquired at intervals of 5° in the multislice ISI mapping method.

To verify the performance of the proposed B_1 mapping method in an *in vivo* human brain, MR experiments were performed, and all analyses conducted with the phantom, except for B_0 correction, were repeated. Figure 7 shows the FA maps of the proposed B_1 mapping method, multislice ISI mapping method, and FA error maps for three slices. In the region-of-interest analysis, differences among the two methods and FA errors were −3.2%, 4.8%, and 6.7%, respectively.

5. Discussion

A novel B_1 mapping method using a pair of composite RF pulses and SER techniques is presented in this study. This B_1 mapping method could improve 3D spatial coverage of B_1 mapping with long TR to reduce the effect of T_1, and its characteristics were confirmed with computational simulations and phantom and *in vivo* human experiments on the 3-Tesla MRI scanner.

In computational simulations, the results revealed that the ANR distribution of the proposed B_1 mapping method is more uniform compared to that of Morrell's method [16], DAM [11], and Yarnykh's method [14]. These results suggest that the proposed B_1 mapping method could provide more accurate B_1 field strength measurements over a wider B_1 field strength range. Additionally, our proposed B_1 mapping method has more acquisition time efficiency compared with Morrell's method [16] by having multiple excitation RF pulses with different RF frequency offsets on the single TR for multislice MR imaging. Such strength of the proposed B_1 mapping method can be applied to Morrell's method [16] because its methodology is similar to that of Morrell's method [16].

In the phantom experiment, the results showed that there was no significant difference in the B_1 field distribution (<10%) between the proposed B_1 mapping method and multislice ISI mapping method. In addition to phantom experiments, the results of the *in vivo* human brain study revealed that the differences between the proposed B_1 mapping method and multislice ISI mapping method were noted at the Gaussian noise level in the FA distribution (<10%). Here, the multislice ISI mapping method was used as a reference method for performance evaluation of the proposed B_1 mapping method due to its accuracy by repeated measurements of signal intensity [8]. Based on these results, the proposed B_1 mapping method facilitates FA distribution with high accuracy and temporal resolution within a single TR, regardless of the tissue characteristics.

However, the proposed B_1 mapping method has several limitations in terms of its narrow bandwidth and restricted

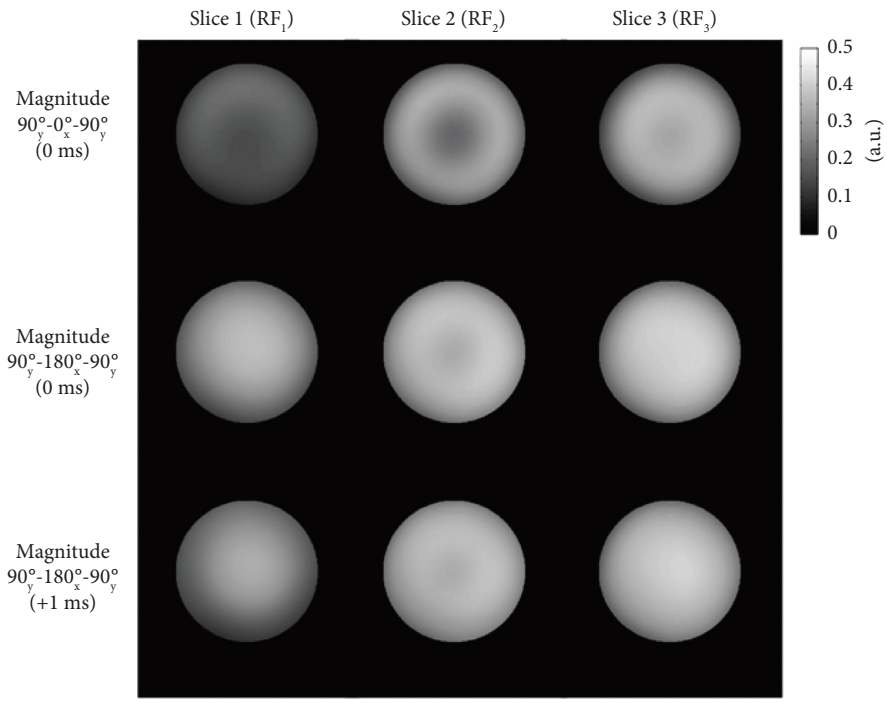

FIGURE 5: MR images for three echo signals, RF_1 (top row), RF_2 (centre row), and RF_3 (bottom row), obtained from the composite RF pulses in the phantom. Here, slices 1, 2, and 3 were obtained at different TEs.

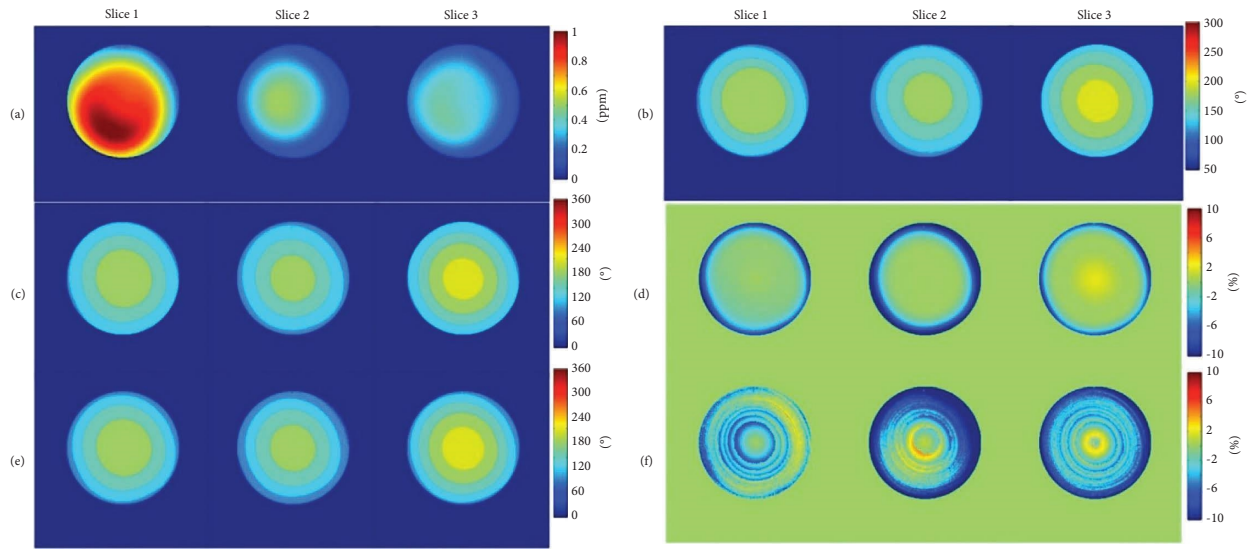

FIGURE 6: Resulting phase of the proposed B_1 mapping method and multislice ISI mapping method with the phantom. (a) B_0 inhomogeneity maps. (b) Resulting phase maps and (c) the resulting phase maps corrected for B_0 inhomogeneity for the proposed B_1 mapping method. (d) Error values before and after B_0 inhomogeneity corrections for the proposed B_1 mapping method. (e) B_1 maps calculated using the multislice ISI mapping method. (f) Error values between the proposed B_1 mapping method and multislice ISI mapping method.

TR in connection with the slice selectivity and number of RF excitation pulses. These limitations can be overcome using a high-power RF amplifier and parallel RF excitation, but the proposed B_1 mapping method can increase the SAR in such situations. Moreover, a multichannel transmission RF coil should be used for parallel excitation in the proposed B_1 mapping method; however, this application is limited in commercial 3-Tesla MRI scanners.

In addition to limitation of the proposed B_1 mapping method, this study has some limitations. First, B_0 correction was not performed in data processing procedure for *in vivo* human brain due to the differences in signal intensity between the proposed B_1 mapping method and multislice ISI mapping method observed at the Gaussian noise level. Moreover, the proposed B_1 mapping method was evaluated in brain region only in this work at 3-Tesla MRI scanners.

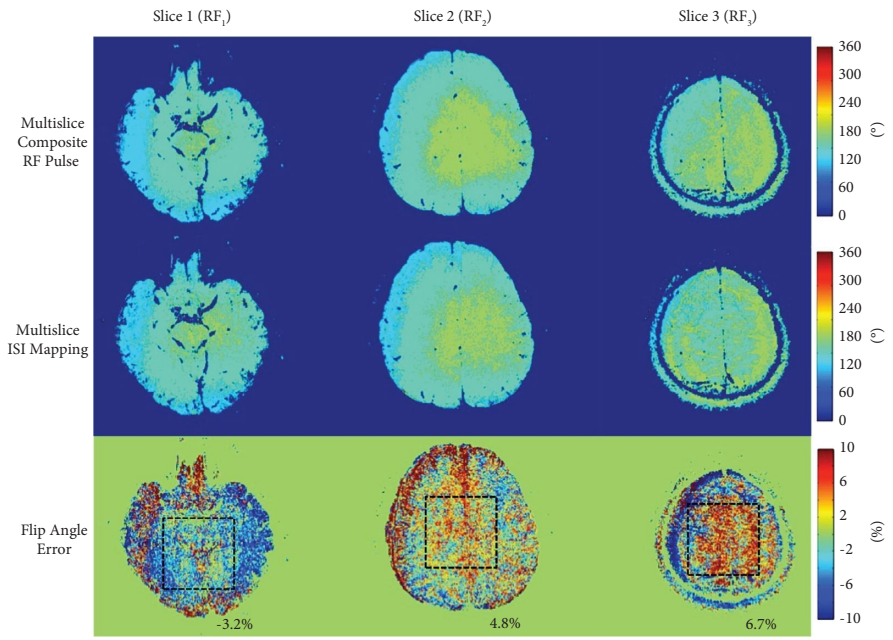

FIGURE 7: FA maps of the proposed B_1 mapping method and multislice ISI mapping method for an *in vivo* human brain and FA error maps for three echo signals (RF_1, RF_2, and RF_3).

However, in a recent report, the proposed B_1 mapping method had been successfully implemented for the whole-body imaging in the 1.5-Tesla MRI scanners, showing the robustness and feasibility of the proposed method [29].

The B_1 mapping method proposed in this study is based on phase-sensitive B_1 mapping methods. Since both double angle and phase-sensitive B_1 mapping methods require moderately long TRs, the imaging speed using one of these methods depends primarily on the acquisition scheme used. Presaturated double angle B_1 mapping with reduced scan time has been achieved using slice-selective excitation and rapid spiral data acquisition [16]. This rapid readout scheme could be applied to the phase-sensitive technique to have a similar effect as reducing acquisition time.

Furthermore, the phase-sensitive B_1 mapping methods could only be applied to 3D imaging, as the RF pulses are nonselective. Nonselective excitation is used to minimize the duration of excitation to allow B_1 mapping over a wide range of B_0 inhomogeneity. Moreover, nonselective excitation necessitates large imaging volumes, which leads to low resolution or long acquisition time. Slab selective excitation with high bandwidth pulses for spatially localized 3D imaging could be implemented in the phase-sensitive method for greater ease and flexibility of scan volume prescription. This would cause some increase in RF pulse length, with some resulting narrowing of the range of B_0 inhomogeneity over which the method is valid [16]. This may be investigated in future work.

For some B_1 mapping applications, severe imaging time constraints may make slice-selective excitation desirable to allow rapid B_1 mapping over a single slice. Implementation of slice-selective excitation in the phase-sensitive B_1 mapping methods would more severely restrict the range of B_0 inhomogeneity over which the method is valid and may not be feasible. Thus, there may be some applications requiring extremely short imaging times where the double angle techniques implemented with slice-selective excitation may be more useful than the phase-sensitive B_1 mapping methods. When there are no significant time constraints, a precise B_1 mapping is performed using a 3D acquisition method, because any slice-selective method of B_1 mapping will include signal from the transition bands of the slice profile, thus causing systematic errors in the estimation of B_1.

In this study, the B_1 mapping method based on phase-sensitive technique using a pair of composite RF pulses and SER techniques can be applied to clinical applications, such as echo-planar imaging and parallel imaging, along with shorter acquisition time. Moreover, this proposed B_1 mapping method does not need to increase T_1 effect by reducing the TR for shorter acquisition time and is suitable for clinical application due to its wide 3D spatial coverage and long TR, so it is possible to obtain an accurate B_1 mapping even if RF spoiling is unstable. Additionally, this proposed B_1 mapping method allows calibration of the receive delivery and enables accurate B_1 mapping.

6. Conclusions

We demonstrated that the proposed B_1 mapping method using a pair of composite RF pulses and SER techniques can reliably measure RF B_1 propagation in a multislice imaging and SER technique, providing the effect of acquisition time reduction and wider 3D spatial coverage of B_1 mapping with long T_1, respectively. Particularly, this B_1 mapping method may be suitable for the B_1 mapping required for accurate FA analysis using high-field MRI scanners.

Data Availability

The experimental data used to support the findings of this study have not been made available due to legal and confidential restrictions under the law by the Korea University Research Foundation.

Disclosure

A portion of this study has been published as a doctoral dissertation by Jeung-Hoon Seo.

Conflicts of Interest

The authors declare that they have no conflicts of interest.

Authors' Contributions

Suchit Kumar and Kyu Chan Lee contributed equally to this work.

Acknowledgments

This work was supported by the Korea Medical Device Development Fund grant funded by the Korea government (the Ministry of Science and ICT, the Ministry of Trade, Industry and Energy, the Ministry of Health & Welfare, and the Ministry of Food and Drug Safety) (Project numbers: 1711138003 and RS-2020-KD000041) and Institute of Information & Communications Technology Planning & Evaluation (IITP) grant funded by the Korea government (MSIT) (grant no. 1711160590, Development of digital twin based real-time untact cardiovascular disease prediction and monitoring technology).

References

[1] U. Katscher, P. Börnert, C. Leussler, J. S. van den Brink, and S. E. N. S. E. Transmit, "Transmit SENSE: transmit SENSE," *Magnetic Resonance in Medicine*, vol. 49, no. 1, pp. 144–150, 2002.

[2] Y. Zhu, "Parallel excitation with an array of transmit coils," *Magnetic Resonance in Medicine*, vol. 51, no. 4, pp. 775–784, 2004.

[3] D. Xu, K. F. King, Y. Zhu, G. C. McKinnon, and Z.-P. Liang, "Designing multichannel, multidimensional, arbitrary flip angle RF pulses using an optimal control approach," *Magnetic Resonance in Medicine*, vol. 59, no. 3, pp. 547–560, 2008.

[4] J. B. M. Warntjes, O. D. Leinhard, J. West, and P. Lundberg, "Rapid magnetic resonance quantification on the brain: optimization for clinical usage," *Magnetic Resonance in Medicine*, vol. 60, no. 2, pp. 320–329, 2008.

[5] J.-M. Kim, C. Lee, S.-D. Hong, J.-H. Kim, K. Sun, and C.-H. Oh, "T1-Based MR temperature monitoring with RF field change correction at 7.0T," *Investigative Magnetic Resonance Imaging*, vol. 22, no. 4, p. 218, 2018.

[6] J. P. Hornak, J. Szumowski, and R. G. Bryant, "Magnetic field mapping," *Magnetic Resonance in Medicine*, vol. 6, no. 2, pp. 158–163, 1988.

[7] S. Akoka, F. Franconi, F. Seguin, and A. Le Pape, "Radiofrequency map of an NMR coil by imaging," *Magnetic Resonance Imaging*, vol. 11, no. 3, pp. 437–441, 1993.

[8] E. K. Insko and L. Bolinger, "Mapping of the radiofrequency field," *Journal of Magnetic Resonance, Series A*, vol. 103, no. 1, pp. 82–85, 1993.

[9] R. Stollberger and P. Wach, "Imaging of the active B1 field in vivo," *Magnetic Resonance in Medicine*, vol. 35, no. 2, pp. 246–251, 1996.

[10] J. K. Maier, G. H. Glover, and L. M. Arana, "Method for mapping the rf transmit and receive field in an nmr system," General Electric Company, Milwaukee, WI, USA, US Patent 5001428, 1991.

[11] C. H. Cunningham, J. M. Pauly, and K. S. Nayak, "Saturated double-angle method for rapid B_1^+ mapping," *Magnetic Resonance in Medicine*, vol. 55, no. 6, pp. 1326–1333, 2006.

[12] A. B. Kerr, "Accelerated B1 mapping for parallel excitation," in *Proceedings of the 15th Annual Meeting of ISMRM*, p. 352, Berlin, Germany, January 2007.

[13] N. G. Dowell and P. S. Tofts, "Fast, accurate, and precise mapping of the RF field in vivo using the 180° signal null," *Magnetic Resonance in Medicine*, vol. 58, no. 3, pp. 622–630, 2007.

[14] V. L. Yarnykh, "Actual flip-angle imaging in the pulsed steady state: a method for rapid three-dimensional mapping of the transmitted radiofrequency field," *Magnetic Resonance in Medicine*, vol. 57, no. 1, pp. 192–200, 2006.

[15] F. Jiru and U. Klose, "Fast 3D radiofrequency field mapping using echo-planar imaging," *Magnetic Resonance in Medicine*, vol. 56, no. 6, pp. 1375–1379, 2006.

[16] G. R. Morrell, "A phase-sensitive method of flip angle mapping," *Magnetic Resonance in Medicine*, vol. 60, no. 4, pp. 889–894, 2008.

[17] Y. V. Chang, "Rapid B_1 mapping using orthogonal, equal-amplitude radio-frequency pulses," *Magnetic Resonance in Medicine*, vol. 67, no. 3, pp. 718–723, 2011.

[18] L. I. Sacolick, F. Wiesinger, I. Hancu, and M. W. Vogel, "B_1 mapping by Bloch-Siegert shift," *Magnetic Resonance in Medicine*, vol. 63, no. 5, pp. 1315–1322, 2010.

[19] C. H. Oh, S. K. Hilal, Z. H. Cho, and I. K. Mun, "Radio frequency field intensity mapping using a composite spin-echo sequence," *Magnetic Resonance Imaging*, vol. 8, no. 1, pp. 21–25, 1990.

[20] A. Sharma, S. Tadanki, M. Jankiewicz, and W. A. Grissom, "Highly-accelerated Bloch-Siegert $|B_1^+|$ mapping using joint autocalibrated parallel image reconstruction," *Magnetic Resonance in Medicine*, vol. 71, no. 4, pp. 1470–1477, 2014.

[21] F. Bloch and A. Siegert, "Magnetic resonance for nonrotating fields," *Physical Review*, vol. 57, no. 6, pp. 522–527, 1940.

[22] M. Bouhrara and J.-M. Bonny, "B_1 mapping with selective pulses," *Magnetic Resonance in Medicine*, vol. 68, no. 5, pp. 1472–1480, 2012.

[23] S. Volz, U. Nöth, A. Rotarska-Jagiela, and R. Deichmann, "A fast B_1-mapping method for the correction and normalization of magnetization transfer ratio maps at 3 T," *NeuroImage*, vol. 49, no. 4, pp. 3015–3026, 2010.

[24] F. Balezeau, P.-A. Eliat, A. B. Cayamo, and H. Saint-Jalmes, "Mapping of low flip angles in magnetic resonance," *Physics in Medicine and Biology*, vol. 56, no. 20, pp. 6635–6647, 2011.

[25] A. C. Rejimon, D. Y. Lee, C. M. Bergeron et al., "Rapid B_1 field mapping at 3 T using the 180° signal null method with extended flip angle," *Magnetic Resonance Imaging*, vol. 53, pp. 173–179, 2018.

[26] J. E. Bishop, D. B. Plewes, and T. E. interleaving, "TE interleaving: n," *Journal of Magnetic Resonance Imaging*, vol. 1, no. 5, pp. 531–538, 1991.

[27] D. A. Feinberg, T. G. Reese, and V. J. Wedeen, "Simultaneous echo refocusing in EPI," *Magnetic Resonance in Medicine*, vol. 48, no. 1, pp. 1–5, 2002.

[28] G. R. Morrell and M. Schabel, "A noise analysis of flip angle mapping methods," in *Proceedings of the 17th Annual Meeting of ISMRM*, p. 376, Hawaii, HA, USA, August 2009.

[29] S. Kumar, H. J. Chung, Y. J. Jeong, H. K. Lee, and C. H. Oh, "Design and implementation of split-leg type elliptical whole-body birdcage RF coil at 1.5 T MRI," *Applied Sciences*, vol. 11, no. 16, p. 7448, 2021.